Check for updates

Spin-induced electron transmission through metal–organic chiral crystals†

Tapan Kumar Das,[a] Amit Kumar Mondal, [ID][ae] Om Shanker Tiwari, [ID][b] Pandeeswar Makam,[b] Gregory Leitus,[c] Ehud Gazit, [ID][b] Fontanesi Claudio [ID][d] and Ron Naaman [ID] *[a]

Metal–organic Co(II)-phenylalanine crystals were studied and were found to possess magnetic properties and long-range spin transport. Magnetic measurements confirmed that in the crystals there are antiferromagnetic interactions between Co(II) and the lattice. The metal–organic crystals (MOCs) also present the chirality-induced spin selectivity (CISS) effect at room temperature. A long-range spin polarization is observed using a magnetic conductive-probe atomic force microscope. The spin polarization is found to be in the range of 35–45%.

Introduction

Metal–organic crystals (MOCs) that have two-dimensional chiral structures exhibit interesting magnetic properties.[1,2] However, typically these chiral organic materials have low conductivity.[3,4] Recently, chiral MOCs were studied that show relatively good conduction in addition to excellent magnetic properties. Those systems are better candidates for organic materials-based spintronic applications and quantum devices.[5] An interesting system in this category includes crystals in which the Cu(II) ions are arranged in two-dimensional (2D) layers with either D or L enantiomers of pentafluorophenylalanine. These crystals show thermally activated ferromagnetism.[1,4] Another example is a system that exhibits two-dimensional ferromagnetic behavior and is formed by the assembly of hexacyanoferrate(III) anions and nickel(II) bis-diamino complexes of the chiral ligand trans-cyclohexane-1,2-diamine (*trans*-chxn).[6] This 2D layered structure exhibits ferromagnetism with Curie temperature $T_c = 14$ K.[5] Hence, there is evidence that combining chirality and paramagnetic ions may result in interesting and non-intuitive magnetic properties. A similar effect was observed in chiral non-magnetic inorganic crystals, where current was used to induce magnetization.[7]

The chiral metal–organic crystals show the chiral-induced spin-selective (CISS) effect.[4] In the last two decades, the CISS effect has been studied extensively in many media including different types of chiral molecules and materials.[8] The effect means that the transport of electrons through chiral systems depends on the electrons' spin state. Very high spin polarization (SP), that is larger than 50%, was observed for various type of systems, varying from DNA[9] and oligopeptides[10] to chiral perovskites,[11] supramolecular structures,[12] helicenes,[13,14] and bowl-shaped chiral subphthalocyanines.[15] In all these studies, the SP was defined for measuring the current through the chiral system located between two electrodes, at least one of them made from ferromagnet that can be magnetized either towards (up) or away (down) from the chiral system. The SP% $= \dfrac{I_{up} - I_{down}}{I_{up} + I_{down}} \times 100$

when I_{up} and I_{down} are the currents measured for the magnetic pointing towards or away from the chiral system, respectively.

Here we report MOCs of either L or D-phenylalanine, which were crystallized with Co(II) ions. The Co(II) atoms are arranged in 2D layers (Fig. 1). This layer structure results from the amino and carboxylic groups that form a layered structure containing an ordered layer of cobalt atoms sandwiched between the chiral amino acids. We have studied the magnetic behavior of these highly conducting MOCs and found a long-range electron spin transport through them. The long-range spin transport, observed here, is consistent with several recent studies that observed spin selective transport in chiral system that exceeds hundreds of nanometers.[16]

[a] *Department of Chemical and Biological Physics, Weizmann Institute of Science, Rehovot, 7610001, Israel. E-mail: ron.naaman@weizmann.ac.il*

[b] *The Shmunis School of Biomedicine and Cancer Research, The George S. Wise Faculty of Life Sciences, Tel Aviv University, Tel Aviv 6997801, Israel*

[c] *Chemical Research Support, Weizmann Institute of Science, Rehovot, 7610001, Israel*

[d] *Department of Engineering "Enzo Ferrari," University of Modena and Reggio Emilia, Modena 41125, Italy*

[e] *Institute of Nano Science and Technology (INST), Sector-81, Mohali 140306, Punjab, India*

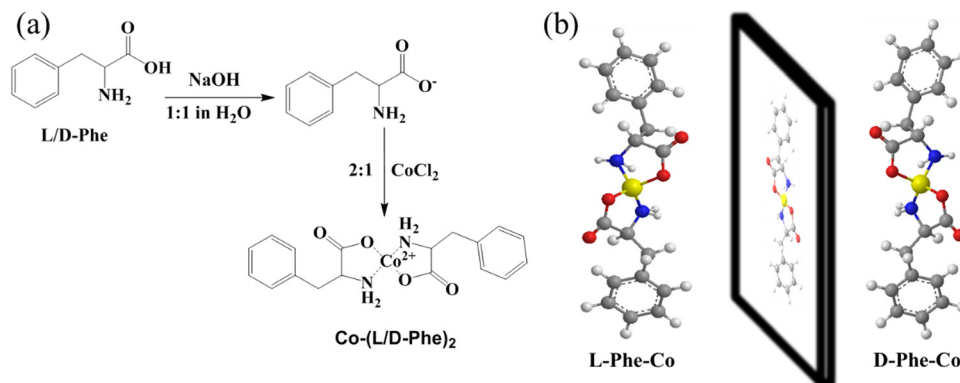† Electronic supplementary information (ESI) available. See DOI: https://doi.org/10.1039/d3cp02579a

Experiment

Sample preparation and characterization

L/D-Phenylalanine-Co crystal fabrication crystals were fabricated by reacting 2 equiv. of L/D-Phenylalanine (10 mM), 2 equivalents

22124 | *Phys. Chem. Chem. Phys.*, 2023, **25**, 22124–22129

This journal is © the Owner Societies 2023

Fig. 1 (a) Molecules and solvents used for the synthesis and the chemical structure of the L/D-Phe-Co^{2+} crystals. (b) An illustration of the Phe-Co^{2+} crystals and their mirror symmetry.

of sodium hydroxide (10 mM), and 1 equiv. of CoCl$_2$ (10 mM) in water at 60 °C. Pink plate-like crystals were formed during the cooling stage. The crystals were filtered off, washed with deionized water, and dried under vacuum.

Both crystals such as L/D-Phe aromatic amino acids with Co^{2+} were crystallized in ultrapure water (Biological Industries, Beit Haemeck, Israel), after which the crystals were filtered and completely dried under vacuum before performing the PXRD experiments. The L/D-Phe-Co crystal powder samples were deposited on a quartz zero-background sample holder. The PXRD pattern was collected using a Bruker D8 Discover diffractometer (Bruker, Germany) equipped with Goebels mirrors to parallelize the beam as well as a LYNXEYE-XE linear detector. Data collection was performed at room temperature at a scan range of 2θ of 2–40°. The optical micrographs of both L/D-Phe-Co crystals were captured by drop-casting crystals on a glass slide, and were directly observed using a Nikon Eclipse Ti-E fluorescence microscope at bright field channels.

Optical and magnetic characterization

UV-Vis measurements of the L/D-Phe-Co complex were performed using a Cary Series UV-Vis spectrophotometer (model Cary 100 UV-Vis; Agilent Technologies). A quartz cuvette with an optical path length of 1 mm was used for all the measurements. CD spectroscopy studies of the L/D-Phe-Co complex were carried out on a Chirascan CD spectropolarimeter using a cylindrical, jacketed quartz cell (a path length of 10 mm) connected to a Julabo-UC25 water circulator. The wavelength range was 190 nm to 300 nm. For reproducible data, each set of spectra was measured using at least three individually prepared solutions. CD spectra were recorded using a spectral bandwidth of 1.0 nm at 25 °C with a time constant of 1 s and a step resolution of 1 nm. All spectra were recorded in water and typically averaged over 3–5 scans. A quartz cell with a path length of 1 mm was used with solutions containing approximately 0.25 mL. All the spectra were obtained following solvent background subtraction.

The magnetometry was performed by using a MPMS3 SQUID magnetometer (LOT-Quantum Design, Inc.) by applying a vibrating sample mode. The measurement was done by placing the sample in a standard brass holder. The temperature-dependent magnetic susceptibility and the magnetic moment were taken by cooling samples to 2 K under a 1000 Oe magnetic field and again samples were measured while heating from 2 to 300 K. The magnetic field dependencies were taken at different temperatures in intervals while the magnetic field H was decreased and increased in the range -60 kOe $\leq$ H $\leq$ $+60$ kOe.

Magnetic conductive atomic force microscopy (mc-AFM)

The crystal was placed on a Si/SiO$_2$ wafer coated with 8 nm Ti, 100 nm Ni, and 8 nm Au. Magnetic-field-dependent currents *versus* the voltage (*I–V*) characteristics of the crystals were obtained using a multimode magnetic scanning probe microscopy system built with Beetle Ambient AFM and an electromagnet equipped with a R9 electronic controller (RHK Technology). *I–V* measurements were performed by applying voltage with Pt tip (DPE-XSC11, µmasch with a spring constant 3–5.6 N m^{-1}) in contact with the crystal at an applied force of 5 nN. More than 50 *I–V* curves were scanned for both the magnetic field direction, *i.e.*, the magnetic field in the up and down direction perpendicular to the substrate and the crystal surface.

Results and discussion

The Phenylalanine MOCs were separately crystallized with Co(II) ions and the plate-like chiral crystals were formed at 60 °C. Highly pure materials were used for the synthesis of Phe-Co crystal, to rule out any contribution from impurities. A schematic of the complex formation is shown in Fig. 1a, whereas the crystal structures of both enantiomers are shown in Fig. 1b. To unravel the crystal structure, powder X-ray diffraction (PXRD) studies were performed. The PXRD patterns for both L/D-Phe-Co crystals are shown in Fig. 2a. Both samples exhibited highly crystalline structures confirmed by the reflection peaks at 2θ. The unit cells and the ordered layers of the cobalt atoms located between the amino acids are shown in Fig. 2b. The structure of the crystals belongs to a noncentrosymmetric space group, $P2_1$. The asymmetric units of both helices of Co(II)-Phe comprise an amino acid dimer coordinating a Co-atom. The crystals have layered structure containing an ordered layer of Co-atoms sandwiched between amino acids (Fig. 2b). In the study, we used crystals with dimensions in the range of 300 to 500 nm.
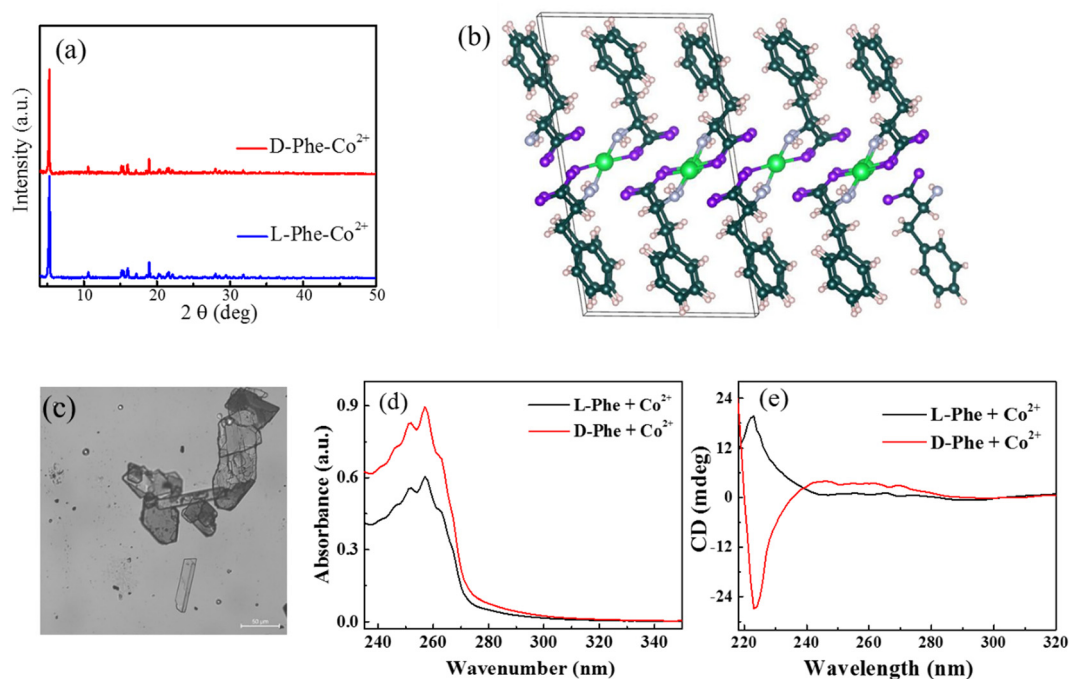
This journal is © the Owner Societies 2023

Phys. Chem. Chem. Phys., 2023, **25**, 22124–22129 | **22125**

Fig. 2 (a) PXRD of both L/D-Phe-Co^{2+} crystals collected using a Bruker D8 Discover diffractometer (b) a schematic crystal structure arranged in 2D layers of Phenylalanine. (c) Optical micrograph of L-Phenylalanine Co^{2+} crystal. (d) Optical absorption and (e) Circular Dichroism (CD) spectra of both L/D-Phe-Co^{2+} crystals.

Optical micrograph imaging also confirmed the plate-like crystal structures (Fig. 2c). We subjected the chiral crystals to optical absorption and circular dichroism (CD) analysis and visualized the optical activity possessed by both MOCs. A set of absorption peaks are seen in the UV region located between the 250 and 275 nm wavelengths (Fig. 2d). The CD spectra exhibited a positive and negative Cotton effect at 222 nm, for the D and L enantiomers, respectively (Fig. 2e). The intensity of the CD peaks for the two enantiomers, are not identical because of the size of the crystals measure, as also verified in the different in the absorption peaks. However, the CD peak intensity divided by absorption is the same for both enantiomers, which means that indeed they have the same asymmetry factor. The crystals of both enantiomers were found to be very stable for a long time and even after 300 days, the CD signals remained unchanged.

The temperature-dependent magnetic susceptibility and the magnetic moment of one-enantiomer (L-Phe-Co) were measured using a superconducting quantum interference device (SQUID). The magnetic susceptibility was measured as a function of temperature under an applied field of 1000 Oe (Fig. 3a) and the magnetic moment as a function of the magnetic field applied perpendicular to the *ab* crystal plane (Fig. 3b). The product of the molar magnetic susceptibility and the temperature χT is 1.9 cm^3 Kmol^{-1} at 300 K. This value steadily decreases with a decrease in temperature and reaches a value of 0.9 cm^3 Kmol^{-1} at 1.9 K. This value corresponds to the theoretical value of the Curie constant C_{Co}^{2+} = 1.87 cm^3 Kmol^{-1} calculated (see eqn (1S), ESI†) for the Co^{2+} ion in the 3d^7 electronic configuration with the $^4F_{9/2}$ ground state. This behavior of χT as a function of temperature indicates the presence of antiferromagnetic interactions between the Co^{2+} ions in the crystal lattice. Fig. 3b and c present the
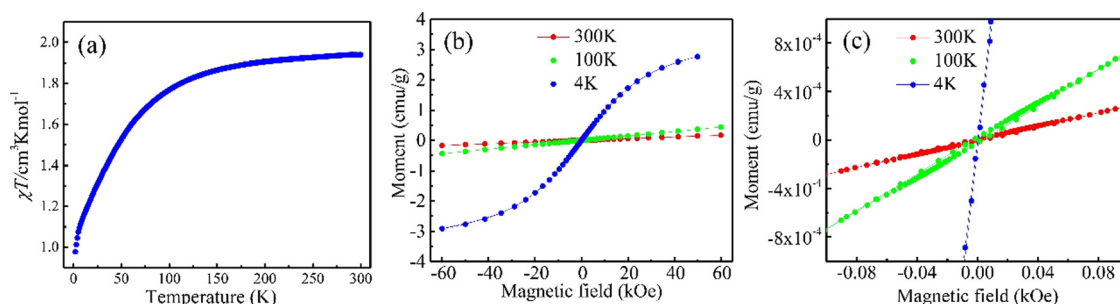

Fig. 3 Magnetic properties of L-Phe-Co crystals measured parallel to the crystal *ab* surface. (a) Temperature-dependent magnetic susceptibility χ, (b) and (c) full spectrum of the magnetic moment as a function of the applied magnetic field for three different temperatures.

22126 | *Phys. Chem. Chem. Phys.*, 2023, **25**, 22124–22129

This journal is © the Owner Societies 2023

magnetic moment as a function of the applied field. A strong predominant paramagnetic response decreases with temperature. No hysteresis in the magnetization curve could be observed throughout the temperature range; however, the drastic change in magnetization at lower temperatures indicates the importance of the interaction of the ion atoms with the crystal lattice. The interaction of the metal ion with the chiral organic lattice by spin exchange, was observed before in the case of the Cu-phenylalanine.[1] It was explained there based on calculations that demonstrated indirect spin exchange interaction between the metal ions through the lattice. However, while there this spin exchange interaction led to ferromagnetism that increased with temperature, here it is antiferromagnetic in nature, probably due to the slight change in the crystal structure.

Similar to the Cu-phenylalanine crystals[1] the Co ions, like the Cu ions enable electrons conduction through the crystals. Electrical measurements were performed for the L enantiomer of the Phe-Co crystal in a planar architecture in a four-point contact configuration. This device configuration allows the conduction to be measured in the *ab* plane of the crystals (Schematic Fig. 4a, inset). The temperature-dependent surface resistivity shown in Fig. 4a is similar to a metal-insulator transition. The resistivity is high at temperatures below ∼40 K, whereas at higher temperatures, above 100 K, it shows Arrhenius-type behavior (Fig. 4b). The activation energy was estimated by extrapolating the linear region from $\log(\rho)$ *versus* the inverse of temperature and was found to be 64 meV. The temperature-dependent current–voltage characteristic curves are shown in Fig. 4c; they confirm that there is a systematic increase in current with an increase in temperature. This behavior is indeed expected for semiconductors with a relatively narrow gap.

The spin-selective electron transmission through both enantiomers of the Phe-Co crystals was studied by mc-AFM, shown schematically in Fig. 5a. The measurements probe the spin selectivity of the chiral crystals along with the effect of the interface between chiral crystals and the ferromagnetic surface. The crystals of both L/D-Phe-Co were transferred to a gold-coated nickel surface (Au/Ni) and the surface was magnetized with magnetization perpendicular to the surface, with a magnetic north pole pointing either up or down. The silicon oxide serves as insulating smooth substrate, Ni is the ferromagnetic layer

that is injecting spin polarized electrons according to the magnetization direction dictated by an external magnet, and the thin gold layer serves for protecting the Ni from being oxidized, while allowing spin-polarized electrons to pass through it.[17] Before obtaining the current–voltage characteristic curve, the morphology of both crystals was analyzed using an AFM topography image. Then the current–voltage (I–V) curves were obtained and each plot shown represents the average of about 50–60 I–V scans. The spin-dependent conduction is measured through crystals of a thickness exceeding 150 nm. The magnitude of the current is higher for D-Phe-Co crystals when the magnet is down and lower when the magnet is up (Fig. 5b) and the opposite behavior is observed for L-Phe-Co crystals (Fig. 5c). It is important to appreciate that the two crystals (L and D) are not identical in the dimensions and therefore the plots are not exactly mirror images of each other. The SP (%) of both helixes is in the range of 35–45% at room temperature (Fig. 5d). These values are very high considering the conduction length and the fact that the measurements are performed at room temperature. As the semi-log plots in the inserts in Fig. 5a and b indicate, there is a different injection threshold for the two spins. This means that there are different barriers for injecting each of the spins, with the different in barrier height of about 100–200 meV. From these two figures, it is possible to conclude that the conduction is not linear with the applied voltage and that the barrier is not solely due to spin orbit coupling (SOC), since in any plausible scenario the SOC should be at least an order of magnitude smaller. It was proposed that this difference relates to the properties of the interface.[18–20]

The noisy spin polarization curves in Fig. 5d is a result of the crystals' surfaces not being smooth which results in large variation of current measurements. However, outside the range of −1 V to +1 V, the spin polarization is certainly above 20%.

Conclusions

MOCs of L/D-Phe were crystallized as enantiopure crystals containing Co(II) ions arranged in 2D layers. The electrical and magnetic measurements demonstrate that the MOCs of Phe-Co^{2+} have good conduction at room temperature and that an antiferromagnetic interaction exists between the metal ions
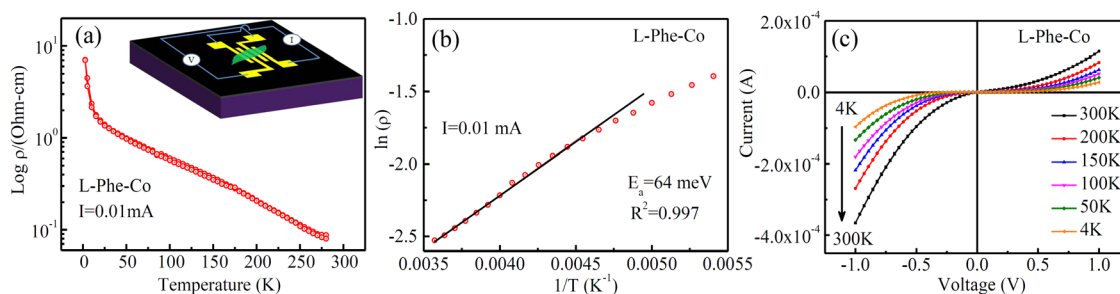

Fig. 4 The electrical properties of the L-Phe-Co crystals. (a) Resistivity measured as a function of temperature in the log scale for an input current of 0.01 mA; the inset shows a schematic of the four-point probe device. (b) Arrhenius plots show the resistivity *versus* the inverse temperature. The activation energy, $E_a = 64 \pm 2$ meV, was calculated by multiplying the slope by the Boltzmann factor. (c) The current–voltage characteristic curves for different temperatures.

This journal is © the Owner Societies 2023

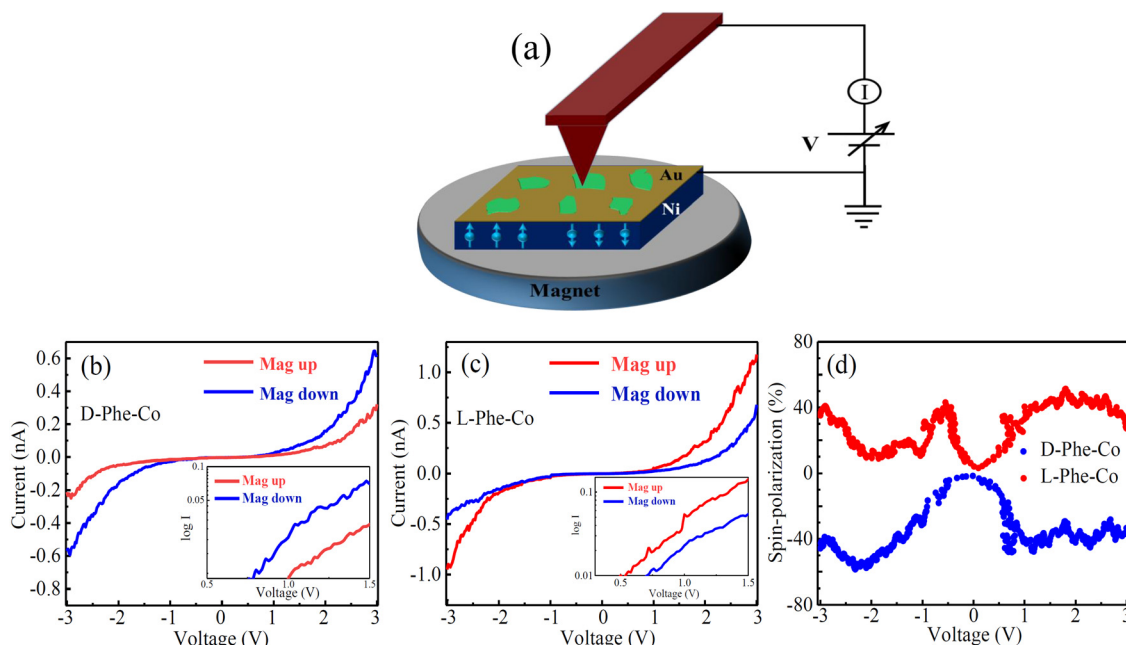*Phys. Chem. Chem. Phys.*, 2023, **25**, 22124–22129 | **22127**

Fig. 5 The spin selective electron transport measurement by a magnetic conductive probe AFM (mCP-AFM). (a) Schematic illustration of the mc-AFM measurement setup. The room temperature $I-V$ curves of (b) D-Phe-Co and (c) the L-Phe-Co crystal were measured using mCP-AFM. (d) The absolute value of the corresponding spin-polarization calculated both helixes. The insets in (b) and (c) show the corresponding curves as a log−log plot. The blue curves correspond to the magnet north pole pointing downward, and the red curves correspond to the magnet north pole pointing upward.

in the lattice. The spin selectivity and long-range spin transport observed in MOCs may have interesting implications for spintronics-related technology. The studied crystals indeed display interesting effects resulting from combining paramagnetic ions and chiral lattices.[21] Recently other organic/inorganic systems[22,23] were shown to also have interesting spin-related properties and together with the MOC, they expand the variety of organic molecule-based solids that can serve in spintronics.

Conflicts of interest

There are no conflicts of interest to declare.

Acknowledgements

References

1 A. K. Mondal, N. Brown, S. Mishra, P. Makam, D. Wing, S. Gilead, Y. Wiesenfeld, G. Leitus, L. J. W. Shimon, R. Carmieli, D. Ehre, G. Kamieniarz, J. Fransson, O. Hod, L. Kronik, E. Gazit and R. Naaman, Long-Range Spin-Selective Transport in Chiral Metal-Organic Crystals with Temperature Activated Magnetization, *ACS Nano*, 2020, **14**, 16624.

2 D.-G. Ha, M. Rezaee, Y. Han, S. A. Siddiqui, R. W. Day, L. S. Xie, B. J. Modtland, D. A. Muller, J. Kong, P. Kim, M. Dincă and M. A. Baldo, Large Single Crystals of Two-Dimensional π-Conjugated Metal-Organic Frameworks via Biphasic Solution-Solid Growth, *ACS Cent. Sci.*, 2021, **7**, 104.

3 R. W. Day, D. K. Bediako, M. Rezaee, L. R. Parent, G. Skorupskii, M. Q. Arguilla, C. H. Hendon, I. Stassen, N. C. Gianneschi, P. Kim and M. Dincă, Single Crystals of Electrically Conductive Two-Dimensional Metal-Organic Frameworks: Structural and Electrical Transport Properties, *ACS Cent. Sci.*, 2019, **5**, 1959.

4 L. S. Xie, L. Sun, R. Wan, S. S. Park, J. A. DeGayner, C. H. Hendon and M. Dincă, Tunable Mixed-Valence Doping toward Record Electrical Conductivity in a Three-Dimensional Metal-Organic Framework, *J. Am. Chem. Soc.*, 2018, **140**, 7411.

5 N. Goren, T. K. Das, N. Brown, S. Gilead, S. Yochelis, E. Gazit, R. Naaman and Y. Paltiel, Metal Organic Spin Transistor, *Nano Lett.*, 2021, **21**, 8657.

6 E. Coronado, C. J. Gomez-García, A. Nuez, F. M. Romero and J. C. Waerenborgh, Synthesis, Chirality, and Magnetic Properties of Bimetallic Cyanide-Bridged Two-Dimensional Ferromagnets, *Chem. Mater.*, 2006, **18**, 2670.

7 T. Furukawa, Y. Watanabe, N. Ogasawara, K. Kobayashi and T. Itou, Current-induced magnetization caused by crystal chirality in nonmagnetic elemental tellurium, *Phys. Rev. B: Condens. Matter Mater. Phys.*, 2021, **3**, 023111.

8 Z. Xie, T. Z. Markus, S. R. Cohen, Z. Vager, R. Gutierrez and R. Naaman, Spin Specific Electron Conduction through DNA Oligomers, *Nano Lett.*, 2011, **11**, 4652.

22128 | *Phys. Chem. Chem. Phys.*, 2023, **25**, 22124–22129

This journal is © the Owner Societies 2023

9 A.-M. Guo and Q.-f Sun, Enhanced spin-polarized transport through DNA double helix by gate voltage, *Phys. Rev. B: Condens. Matter Mater. Phys.*, 2012, **86**, 035424.

10 T. Liu, X. Wang, H. Wang, G. Shi, F. Gao, H. Feng, H. Deng, L. Hu, E. Lochner, P. Schlottmann, S. von Molnar, Y. Li, J. Zhao and P. Xiong, Linear and Nonlinear Two-Terminal SpinValve Effect from Chirality-Induced Spin Selectivity, *ACS Nano*, 2020, **14**, 15983–15991.

11 H. Lu, C. Xiao, R. Song, T. Li, A. E. Maughan, A. Levin, R. Brunecky, J. J. Berry, D. B. Mitzi, V. Blum and M. C. Beard, Highly Distorted Chiral Two-Dimensional Tin Iodide Perovskites for Spin Polarized Charge Transport, *J. Am. Chem. Soc.*, 2020, **142**, 13030.

12 C. Kulkarni, A. K. Mondal, T. K. Das, G. Grinbom, F. Tassinari, M. F. J. Mabesoone, E. W. Meijer and R. Naaman, Highly efficient and tunable filtering of electrons' spin by supramolecular chirality of nanofiber-based materials, *Adv. Mat.*, 2020, **32**, 1904965.

13 V. Kiran, S. P. Mathew, S. R. Cohen, I. H. Delgado, J. Lacour and R. Naaman, Helicenes—A New Class of Organic Spin Filter, *Adv. Mat.*, 2016, **28**, 1957–1962.

14 R. Rodríguez, C. Naranjo, A. Kumar, P. Matozzo, T. K. Das, Q. Zhu, N. Vanthuyne, R. Gómez, R. Naaman, L. Sánchez and J. Crassous, Mutual Monomer Orientation to Bias the Supramolecular Polymerization of [6]Helicenes and the Resulting CPL and Spin Filtering Properties, *J. Am. Chem. Soc.*, 2022, **144**, 7709–7719.

15 J. Labella, D. K. Bhowmick, A. Kumar, R. Naaman and T. Torres, Easily Processable Spin Filters: Exploring the CISS-Effect of Bowl-Shaped Chiral Subphthalocyanines, *Chem. Sci.*, 2023, **14**, 4273–4277.

16 K. Shiota, A. Inui, Y. Hosaka, R. Amano, Y. Ōnuki, M. Hedo, T. Nakama, D. Hirobe, J.-I. Ohe, J.-I. Kishine, H. M. Yamamoto, H. Shishido and Y. Togawa, Chirality-Induced Spin Polarization over Macroscopic Distances in Chiral Disilicide Crystals, *Phys. Rev. Lett.*, 2021, **127**, 126602.

17 R. Naaman and D. H. Waldeck, Spintronics and Chirality: Spin Selectivity in Electron Transport Through Chiral Molecules, *Ann. Rev. Phys. Chem.*, 2015, **66**, 263–281.

18 R. Naaman, Y. Paltiel and D. H. Waldeck, A Perspective on Chiral Molecules and the Spin Selectivity Effect, *J. Phys. Chem. Lett.*, 2020, **11**, 3660–3666.

19 S. Alwan and Y. Dubi, Spinterface Origin for the Chirality-Induced Spin-Selectivity Effect, *J. Am. Chem. Soc.*, 2021, **143**, 14235–14241.

20 Y. Wolf, Y. Liu, J. Xiao, N. Park and B. Yan, Unusual Spin Polarization in the Chirality Induced Spin Selectivity, *ACS Nano*, 2022, **16**, 18601–18607.

21 S.-H. Yang, R. Naaman, Y. Paltiel and S. Parkin, Chiral spintronics, *Nat. Rev. Phys.*, 2021, **3**, 328.

22 Q. Qian, H. Ren, J. Zhou, Z. Wan, J. Zhou, X. Yan, J. Cai, P. Wang, B. Li, Z. Sofer, B. Li, X. Duan, X. Pan, Y. Huang and X. Duan, Chiral molecular intercalation superlattices, *Nature*, 2022, **606**, 902.

23 Y. Xu and W. Mi, Chiral-induced spin selectivity in biomolecules, hybrid organic–inorganic perovskites and inorganic materials: a comprehensive review on recent progress, *Mater. Horiz.*, 2023, **10**, 1924–1955.

This journal is © the Owner Societies 2023

Phys. Chem. Chem. Phys., 2023, **25**, 22124–22129 | **22129**